# APPLIED CFD FOR ANALYSING AERODYNAMIC FLOWS AROUND HELICOPTERS

**Philippe Beaumier, Jean-Marc Bousquet**
**ONERA, 92322 Châtillon, FRANCE**
**beaumier@onera.fr**

**Keywords**: *helicopter, aerodynamics, CFD, optimization, aero-elasticity*

## Abstract

*Current CFD applications on helicopters with the ONERA elsA software are presented. A wide range of viscous steady applications are proposed, including the simulation of isolated fuselage, isolated rotor in hover and quasi-steady simulation of a complete helicopter including main and tail rotor effects. The method is also mature enough to analyze unsteady viscous flows for the airloads prediction of isolated rotors in forward flight. Finally, first results of complete helicopter unsteady CFD simulations are presented.*

## 1 Introduction

The on-going progress in computational resources together with the improvement of numerical methods has contributed to the success of Computational Fluid Dynamics (CFD) in Aeronautics. In the field of helicopters, CFD methods are probably not as widely used as for fixed-wing applications, because of many additional difficulties inherent to the helicopter. Among these specificities, one can quote: the natural unsteadiness of the flow-field, the influence of vortical effects, the large variety of flight conditions and the large influence of elastic deformations of the rotating blades. Despite these difficulties, CFD methods are becoming mature enough to help in the analysis of the flow characteristics around helicopters.

The objective of this article is to present current CFD applications related to helicopters performed at the ONERA Applied Aerodynamics Department. Most of the numerical developments and applications presented below have been done in the framework of a common ONERA-DLR research program CHANCE [1], which aims at the unsteady viscous simulation of the complete helicopter. In a first part, the in-house developed CFD solver *elsA* is presented, with emphasis laid on the methods used for helicopter applications. The second part is devoted to quasi-steady applications, allowing the analysis of the flow-field around isolated fuselages, isolated rotors in hover and around a complete helicopter by a steady approach. Examples of unsteady applications are then presented: they concern the prediction of isolated rotors aerodynamics in forward flight including aero-elastic effects, and a first unsteady simulation of a complete helicopter including the main rotor and fuselage.

## 2 Description of the CFD solver *elsA*

Since 1997, ONERA has made a lot of efforts to develop a new CFD solver *elsA* [2], based on an object oriented architecture. This code can now be used for all types of aerospace configurations [3]: aircraft, space launchers, turbomachinary, missiles and helicopters. It solves the compressible Reynolds Averaged Navier-Stokes (RANS) equations based on a cell-centered finite volume technique for structured multi-block meshes. The space discretization is based on the 2nd order Jamesons's scheme with scalar artificial viscosity and Martinelli's correction. The time integration can be made either using a 4 steps Runge-Kutta technique with the addition of an Implicit Residual Smoothing (IRS) phase, or using a backward Euler time integration with

the addition of an implicit LU relaxation technique. For steady flows, the convergence to steady-state is accelerated by local time stepping and multi-grid algorithms. For unsteady flows where time consistency is needed, a dual time step technique (DTS) or the Gear method can be used, which provide a second order time discretization of the equations. These techniques allow the use of large time steps and are particularly recommended for unsteady viscous applications.

In order to ease the mesh generation process for complex configurations, the Chimera technique is very helpful [4]: the RANS equations are solved simultaneously on body fitted grids and on the background grids, while Chimera interpolations are done between the grids, provided that enough overlap is ensured. The Chimera method can also be used to compute the unsteady motion of the rotating blades. In addition, in order to account for the blades elastic deformations, each computational block can be deformed at each time step following the ALE technique [5]; a Geometric Conservation Law (GCL) is used to preserve the free-stream conservation properties.

Many turbulence models can be used in *elsA* for helicopter applications, from simple algebraic mixing length models (Michel, Baldwin-Lomax) to more sophisticated 2-equation models, such as the k-l model of Smith or the k-ω model of Wilcox, without or with the SST correction.

The boundary conditions are the general non-reflecting far-field boundary condition, and either slip (inviscid) or no-slip adiabatic wall (viscous) conditions. Two specific boundary conditions have been developed for helicopter applications. The first one is devoted to the simulation of hovering rotors, for which it is necessary to apply a far-field boundary condition with non-zero velocities at the boundaries, due to the proximity of these boundaries [6]. The second one concerns the quasi-steady simulation of a rotor by an actuator disk [7]: in this case, the effect of the rotor is modeled by additional source terms on the momentum and energy equations, applied on an infinitely flat disk at the rotor location. Two sub-models can be used: an uniform actuator disk where a constant normal force discontinuity is applied, and a non uniform actuator disk where normal and tangential forces are added (their distribution being provided by an external code).

Finally, for configurations with low Mach numbers, low-speed preconditioning of the compressible RANS equations is necessary in order to avoid poor convergence of the computation [8].

## 3 Quasi-steady applications

### 3.1 Isolated fuselage

The computation of the drag generated by an isolated fuselage has been one of the very first challenges of CFD for helicopter applications. This is indeed an important topic, since it can represent up to 40% of the total drag of the helicopter at high speed. During the HELIFUSE EU-funded project, extensive tests of various fuselage geometry were performed in the F1 wind-tunnel up to real flight Reynolds numbers. These high quality data were used to validate the CFD methods [9].

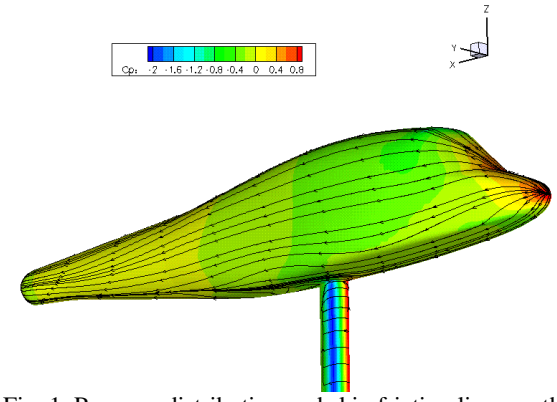


Fig. 1. Pressure distribution and skin friction lines on the C1 HELIFUSE fuselage with strut

Simulations with the *elsA* code of one HELIFUSE test case is presented here: it concerns the C1 geometry at 30 Million Reynolds number, for a free stream Mach number $M_0$=0.235 (Fig. 1). The grid includes approximately 1 Million nodes, and a fully turbulent calculation was done with the k-l

turbulence model. One of the important lessons learnt from HELIFUSE is that the fuselage model support (strut) has to be included in the prediction in order to correctly match the experimental drag values. Another parameter investigated here is the influence of the low-Mach number preconditioning. Table 1 shows that the computation made with the strut provides a 20% increase of the drag coefficient as compared to the calculation without the strut, without or with low-Mach number preconditioning. In addition, although the free stream Mach number is relatively high in the present case, low-speed preconditioning not only has an effect on the quality of the convergence, but also on the fuselage drag values obtained at convergence. In the present case, low-speed preconditioning has an influence in the separated flow regions, behind the strut and at the tail of the fuselage, with subsequent consequences on the total drag values. The drag computation obtained with preconditioning and with the strut is still lower than in the experiment by about 12%.

| | elsA, no precond. | elsA, with precond. | experiment |
|---|---|---|---|
| **w/o strut** | 0.0413 | 0.0386 | - |
| **with strut** | 0.0509 | 0.0462 | 0.0519 |

Table 1. Effect of fuselage strut on fuselage drag coefficient

## 3.2 Isolated rotor in hover

It is well known that hover flight is a dimensioning condition for the helicopter, since the consumed power presents a local maximum in hover, then decreases when the advancing velocity increases up to moderate velocities, before to increase again and exceed the power required for hover flight at high speed. This particular behavior is due to the fact that induced power is maximum in hover. The objective using CFD methods in this case is to be able to capture as accurately as possible the wakes and tip vortices of the hovering rotor in order to predict the induced and viscous losses and as a result the rotor efficiency, characterized by the figure of merit FM.

For an isolated rotor, the solution of the hover problem is steady in the rotating frame of reference. As a consequence, CFD calculations may be done in the rotating frame of reference around one of the rotor blades, the influence of the other blades being accounted by periodicity conditions.

### *3.2.1 Power prediction capabilities*

The validation of CFD prediction is difficult as there is a lack of hover reference test cases with a complete high quality dataset. In the present application, the 7AD 4-bladed model rotor tested in an outdoor facility at Eurocopter Marignane is considered. Only global quantities such as loads and total power are available from these tests, for different blade pitch angles. For the *elsA* calculations a C-H mono-block grid with approximately 750,000 nodes is used.

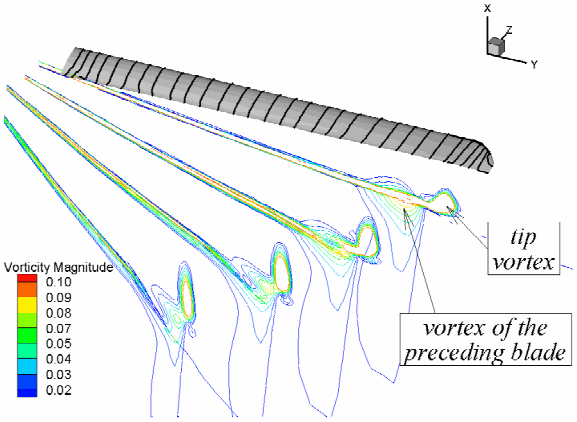


Fig. 2. Field vorticity and blade skin friction lines of the 7AD hovering rotor (k-ω+SST)

For this hovering rotor, Fig. 2 shows very clearly the tip vortex and the shear layer generated by the blade and the vortex of the preceding blade, plotted in different vertical planes located behind the blade; the wake contraction is also captured.

To assess the ability of the *elsA* code to predict the consumed power, the rotor efficiency FM is plotted versus the non-dimensional rotor thrust coefficient Zb in Fig. 3. Results obtained with the k-ω Wilcox turbulence model under-predict the FM, because too high levels of turbulence are generated. A significant improvement is obtained by adding the SST

correction in the k-ω model: the FM values are in better agreement with experiment, at least up to Zb=20. Beyond this value, the calculations become unsteady, as illustrated by the error bars in Fig. 3, because of the apparition of separated flows near the blade tip, which generate a sudden loss of FM. This trend is also obtained in the experiment, but for higher thrust levels (Zb>22). Improvements of the prediction can be expected by a future modeling of the laminar-turbulent transition and the use of refined grids.

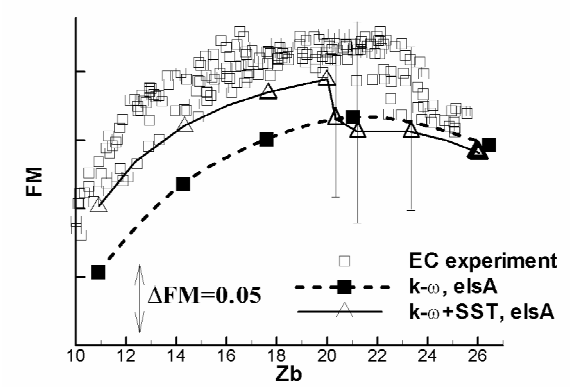


Fig. 3. Influence of turbulence models on Figure of Merit prediction. 7AD rotor in hover

*3.2.2 Influence of blade roots*

CFD can also be used to analyze specific aspects of the flow-field for some flight conditions or geometry where experiment is not easy. A study has been initiated at ONERA to get a better understanding of the flow-field around the blade roots, which are often neglected in isolated rotors computations. One of the objectives of this study is to check the validity of the "hub correction procedure" used in wind-tunnels. Among other parameters, each point of a wind-tunnel test matrix is defined by the thrust and propulsive forces that the aerodynamic part of the rotor blades have to ensure; since these forces exclude the hub and the blade roots, it is required to perform preliminary tests without rotating blades but with only rotating blade roots (also called stubs). The actual forces developed by the aerodynamic part of the blades are then assumed to be the difference between the forces acting on the rotating blades and the forces acting on the rotating stubs. This neglects possible interaction effects. Only CFD can assess the validity of this procedure. In a first step, the numerical study was devoted to hover conditions [10], where computations were performed on isolated blades (without stubs), isolated stubs and the full configuration with blades and stubs. Significant differences were found concerning the flow-field on the isolated stub and on the stub with the rotating blades, as shown in Fig. 4. Separated area of significant extension are observed on the stub with the blade (Fig. 4, right), which are not present on the isolated stub (Fig. 4, left).

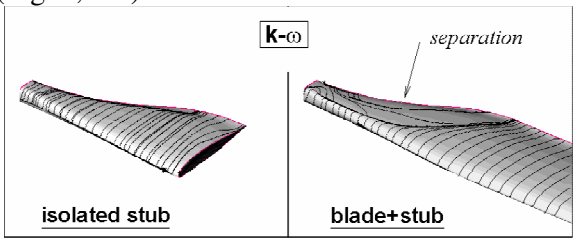


Fig. 4. Skin friction lines in the root blade area for a hovering rotor

The reason for such differences lies on the 3D effects present at the tip of the isolated stub, which are very similar to what can be observed at the tip of a blade. Despite these differences, the validity of the hub correction procedure has been found to be correct in hover condition with an accuracy better than 1% on the rotor forces. Future work will concern the same study in forward flight, where the hub correction procedure can be questioned, especially as far as the drag force generated by the stubs is concerned. An outcome of this study could be an optimization of the shape of the stubs, in order to reduce the consumed power.

*3.2.3 Numerical optimization*

CFD methods used to predict the hovering rotor performance have become efficient enough to be coupled to numerical optimization tools. Indeed, one computation on a coarse viscous grid including 200,000 nodes requires 400 s on a NEC SX5 computer. The optimizer used here is the CONMIN code, which is based on an efficient gradient method, where gradients are solved by finite differences at each optimization iteration. Three descent steps are performed per iteration to search for the objective function

minimum with respect to the constraints by a feasible direction method (projection of the design vector).

The optimization chain is designed to optimize the following parameters defining helicopter rotor blades shape: chord, sweep, anhedral and twist distribution, as well as airfoils position. The blade collective pitch angle is added in order to control the rotor thrust. The objective function is a linear function of the rotor Figure of Merit FM. Constraints can be added if necessary, but most of the applications have been done without any constraints. In this case, the optimizer converges to a rotor geometry with the best maximum FM value, according to the bounds on the design variables provided by the user.

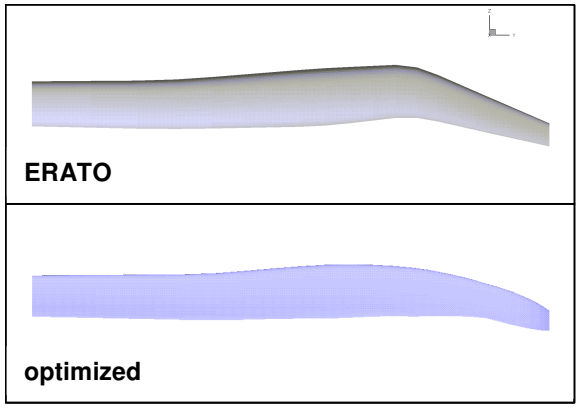


Fig. 5. Reference (ERATO: top) and example of optimized rotor (bottom)

Several applications have been done with this method [11]. As an example, starting from the ERATO blade geometry (Fig. 5, top) designed by ONERA and DLR for aero-acoustic purposes [12], optimization of the blade shape was performed, using 8 design variables, allowing all possible modifications of the blade shape, except the airfoils location which remained unchanged. The optimized geometry is shown in Fig. 5, bottom.

Since the optimization is carried out on coarse grids, a systematic check of the final computation is done on fine grids. In the present case, it was shown that the optimized blade provides a very significant increase of the maximum FM, by almost 5 counts, as illustrated in Fig. 6. Most of the improvements are due to an increase of the blade twist and an increase of the anhedral angle near the blade tip. The next step will be to couple the optimization chain to an aero-mechanic tool to compute the rotor performance in forward flight, in order to perform multi-objective optimization.

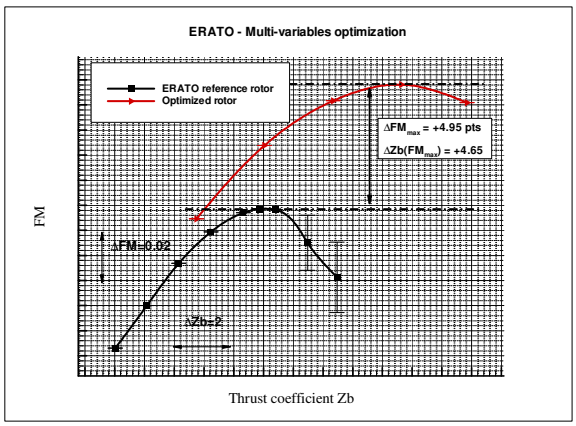


Fig. 6. FM improvement by numerical optimization

### 3.3 Interaction problems

The study of the interactions between the main rotor and the fuselage can be simplified if only quasi-steady effects are considered. In this case, the main rotor can be modeled by an actuator disk, which models only the mean effect of the rotor: the blades passage is of course neglected in this approach. This method has been applied to analyze the flow-field around a Dauphin 365N model helicopter extensively tested in the S2Ch and F1 ONERA wind-tunnels [7]. The results presented here correspond to a test condition defined by the following parameters: advancing speed $V_0$=15 m/s ($M_0$=0.044), Reynolds number Re=1.07 $10^6$ $m^{-1}$, incidence $\alpha$=-3°.

The mesh for viscous calculations has been constructed at ONERA with the ICEM-CFD software. The CAD geometry was simplified (Fenestron removed, simplification of the engines fairing geometry, no modelization of the strut and of the rotor hub). The Navier-Stokes grid is built with a plane in place of the rotor, where the actuator disk condition is applied. The finest grid has a total of about 7 Million points distributed in 97 blocks. The

coarse grid has been obtained by taking one another point in all directions and has a total of about 1 Million points. Computations were first done on the coarse grid without and with main rotor effects to check the actuator disk model. The non-uniform forces distribution used as an input to the actuator disk model were obtained by a trim analysis with a dynamics comprehensive code. The contour lines of stagnation pressure ratio $(\frac{p_i - p_{i0}}{p_{i0}})$ are illustrated in Fig. 7.

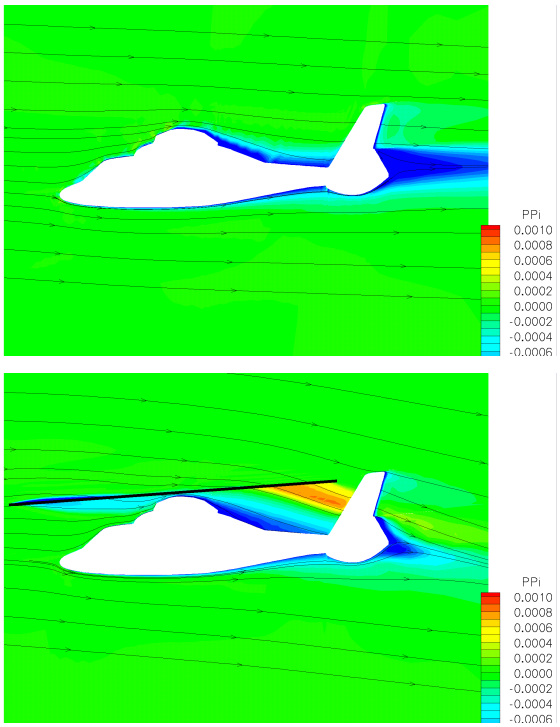


Fig. 7. Flow-field around the fuselage without main rotor (top) and with actuator disk (bottom)

Without the main rotor, a decrease of stagnation pressure is generated behind the engine fairing and behind the tail, due to separated flows. The main rotor creates an increase of stagnation pressure downstream the rotor and a deflection of the flow downwards. This modifies the pressure distribution on the fuselage surface, as illustrated by Fig. 8: the main differences between the isolated fuselage calculation and the calculation with the actuator disk can be seen on the upper part of the tail-boom which experiences higher pressure levels with the main rotor effect, as a consequence of the rotor downwash. The pressure levels are also significantly increased on the horizontal empennage and on the vertical tail surfaces.

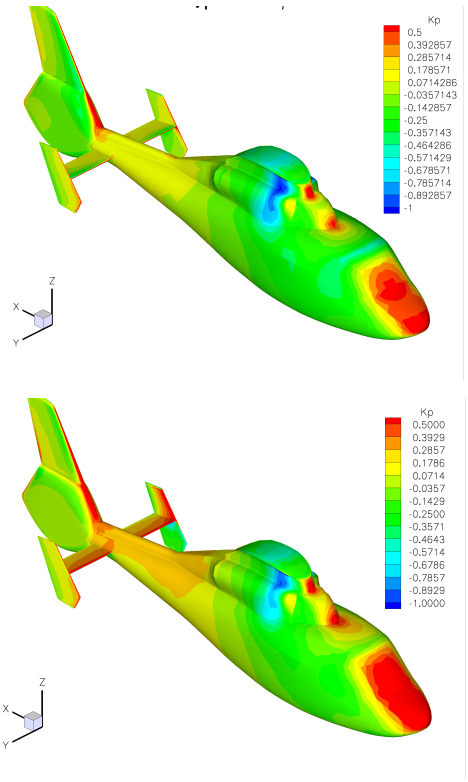


Fig. 8. Pressure distribution on the fuselage without (top) and with (bottom) main rotor modeling

The influence of the rotor downwash on the fuselage global forces and moments is also significant, especially on the drag and on the pitching moment, as discussed in [7].

A comparison of the measured and computed vorticity contour levels in a vertical plane crossing the tail boom is presented in Fig. 9. The experimental values are derived from velocity measurements using a 5-hole probe. The computation with the main rotor effect provides a reasonable agreement with experiment. The vortices emitted at the edge of the rotor disk are well captured by the actuator disk model, with a non symmetric effect between the advancing and retreating sides of the rotor disk, thanks to the non uniform actuator disk model.

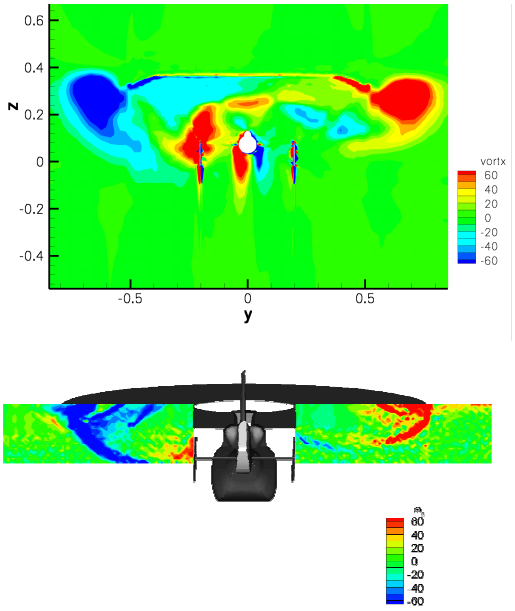


Fig. 9. Comparison of x-component of vorticity: calculation with actuator disk (top), experiment (bottom)

The next step in the simulation of the complete helicopter is the interaction between the fuselage and both the main and tail rotors modelled by the actuator disk formulation. This application was done around a simplified Dauphin configuration with its main rotor and its Fenestron: the empennages are removed and the top of the engine fairing is simplified. In order to ease the grid generation, the mesh of this scale 1 configuration is made of two grids: the background grid includes the fuselage and the fenestron area; an overlapped grid models the main rotor by an actuator disk thanks to the Chimera method implemented in *elsA*. The background grid contains about 5.4 Millions cells distributed in 72 blocks. The computations are made in climb flight conditions ($M_0$=0.1136, α=-11.9°, β=-0.9°). For these conditions, the calculation shows that the downwash of the main rotor directly interacts with the Fenestron. A detailed analysis of the flow-field inside the Fenestron shows a recirculation area in the upstream part of the Fenestron (Fig. 10).

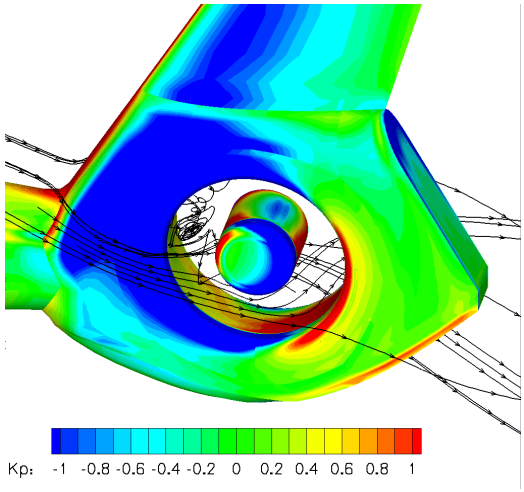


Fig. 10. Flow interaction study in the Fenestron vein. Rotors modeled by actuator-disks

This unconventional flow-field results from the Fenestron thrust which is relatively low in climb flight. A more detailed analysis of the flow-field in the Fenestron is currently underway with an unsteady simulation accounting for the Fenestron rotor blades and stator.

## 4 Unsteady applications

### 4.1 Isolated rotor in forward flight

The simulation of an isolated rotor in forward flight is made difficult not only due to the natural unsteadiness of the flow-field, but also because of the complex blade kinematics. Indeed, the helicopter rotor blades are most of the time articulated in flap, lead-lag and pitch directions, so that each blade has a relative motion with respect to the other blades. Furthermore, helicopter rotor blades have a high aspect ratio (from 12 to 16) and are made of composite materials, so that they can undergo significant elastic deformations, especially torsion deformations. It is widely admitted that a CFD calculation of a realistic helicopter rotor has to account for both rigid and elastic degrees of freedom.

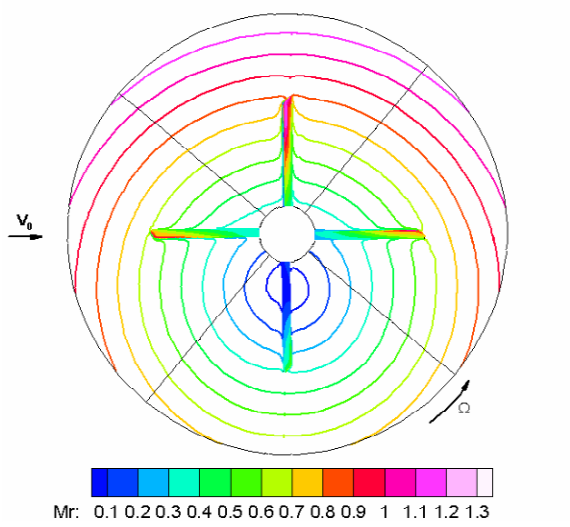


Fig. 11. Relative Mach number contours on the 7AD rotor blades in forward flight ($\mu$=0.4; $M_{TIP}$=0.646)

To simplify this difficult fluid-structure coupling, the CFD simulation can be done with prescribed blade deformations, generally obtained as a result of a trim analysis done with a dynamic comprehensive code. A typical result of an inviscid calculation using this approach is illustrated in Fig. 11, representing contours of the relative Mach numbers on the blades surface and in the plane of rotation. This simulation has been done at a high advance ratio ($\mu$=0.4), for which transonic flows are present on the advancing blade, as shown by the red colors in Fig. 11. The zone of low Mach numbers in the inner part on the retreating blade is also visible by the blue colors: it corresponds to the well-known reverse flow circle.

A detailed study of the influence of viscous effects in the simulations has been done on the 7AD rotor, as illustrated in Fig. 12 which represents the distribution of sectional lift coefficients (top) and sectional pitching moment coefficients (bottom). The Euler results are located on the left, the Navier-Stokes results on the right and the experiment in the middle of the figure. The algebraic turbulence model of Michel has been used in the Navier-Stokes calculations. The experimental values have been obtained by pressure integration of measurements made with a total of 100 unsteady pressure transducers distributed in 5 blade sections. The lift distributions obtained with Euler or Navier-Stokes results are in a reasonably good agreement with experiment: the area of maximum loading in the front and rear parts of the rotor disk are well represented (red colors). However, the area of negative loading on the advancing side at the blade tip, which is typical of high speed flight conditions, is not pronounced enough in the calculations: a slight improvement is obtained with the Navier-Stokes analysis, even if this area of negative loading remains shifted in phase compared to the experiment. The viscous effects have a much more pronounced influence on the pitching moments than on the loads: the Navier-Stokes analysis gives a better prediction of the negative pitching moments in the inner part of the rotor disk. Indeed, in this part, the Euler pitching moments are generally positive, whereas they are strongly negative in the experiment and in the Navier-Stokes analysis.

However, the agreement with experiment is only fair, even with the Navier-Stokes analysis. Improvements of the simulations can be expected thanks to advanced fluid-structure coupling methods. This problem has been addressed for several years in the frame of the CHANCE project. The first method, called weak coupling, mainly aims at providing a trimmed solution at the end of the CFD calculations. As shown in [13], this iterative method converges after only a few iterations. However, the Euler calculations done in [13] showed only limited improvements brought by the coupling method. A second method consists in a time-accurate coupling between the aero-elastic analysis and the aerodynamic CFD analysis: the interest of this method, tested in Euler mode in [13], will be studied in a near future at ONERA using a Navier-Stokes analysis. It is expected that this time accurate coupling should improve the aero-elastic blade response and the corresponding airloads distribution.

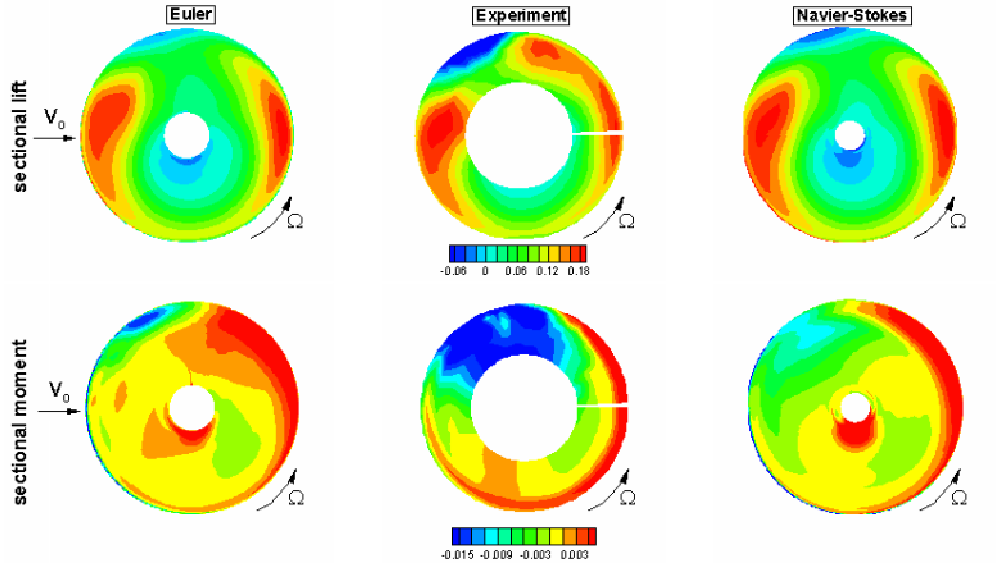


Fig. 12. Sectional loads and moment distributions. Euler (left), experiment (middle), Navier-Stokes (right)

## 4.2 Rotor-fuselage unsteady interactions

The ultimate goal of the CHANCE project is to perform unsteady viscous simulation of a complete helicopter, including main and tail rotor effects. In a first step, the problem was addressed in Euler mode, using a coarse grid with about 1.8 $10^6$ nodes. A view of the body fitted grids around each of the four blades of the Dauphin helicopter model and the background grid around the fuselage is presented in Fig. 13.

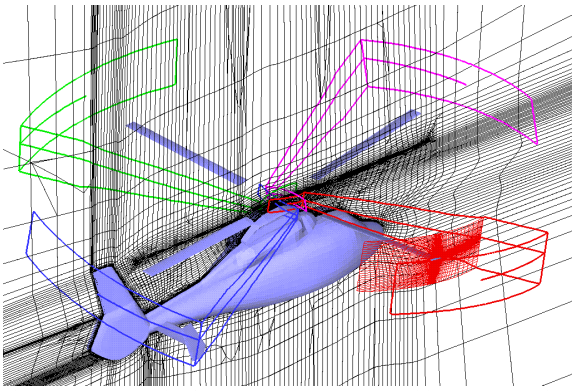

Fig. 13. Euler grid for the complete Dauphin computation

As a first approximation, the blades were assumed to be rigid. The *elsA* calculation used a physical time step corresponding to $\Delta\psi$=0.6°. A periodic solution was obtained after 3 rotor revolutions. The pressure distribution on the fuselage and on the blades for one azimuth angle is illustrated in Fig. 14. High pressure gradients in the front part of the fuselage are observed. The non symmetric solution is clear when looking at the two opposite blades on the advancing and retreating sides of the rotor disk. Furthermore, a dissymmetry appears between the right and left horizontal surfaces in the rear part of the fuselage.

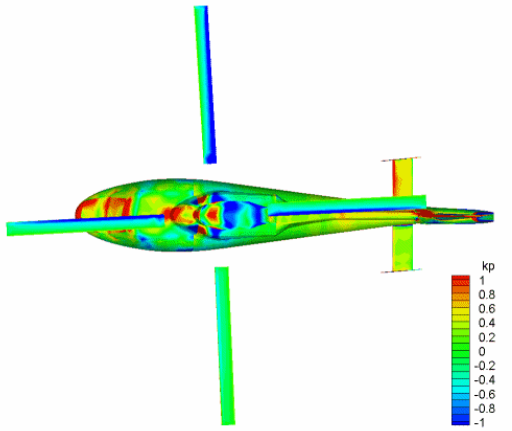


Fig. 14. Unsteady Euler computation of the complete Dauphin helicopter

A quantitative analysis of the unsteady pressure fluctuations generated by the blades passage on the tail boom is currently in progress by comparison of the CFD results with the wind-tunnel results.

## 5 Conclusion and future works

Steady and unsteady CFD applications have been presented for the different fields of helicopter aerodynamics. For steady flows, the numerical methods are efficient enough to perform viscous simulations on realistic configurations such as isolated fuselage, rotor in hover or complete helicopter with actuator disks to model the rotors. For these configurations, most of the differences observed between experiment and simulations are due to inaccurate prediction of separated flows, for which turbulence models are not always adapted. Coupled with an optimization software, the *elsA* code is an excellent design tool for helicopters. The CFD methods are now ready to investigate unsteady flows, despite the considerable amount of CPU time required for such analysis. Following the present unsteady Euler simulations of a complete helicopter, the *elsA* RANS solver will be used for the viscous application before the end of year 2004. In the field of Fluid-Structure coupling, additional work is needed to improve the airloads prediction capabilities.

Despite the considerable progress done during the last decade, CFD is not ready for some particular aerodynamic applications. A first example is the computation of Blade-Vortex Interaction noise, where the numerical methods are not yet accurate enough to capture the blade tip vortices over distances large enough for acoustic applications. The second example is dynamic stall occurring in the retreating blade where LES methods might be of great help to investigate why current CFD methods fail in predicting this complex phenomenon. ONERA is currently preparing solutions to these aerodynamic challenges on the helicopters of the next decade.

## References


[1] D'Alascio A, Pahlke K, Castellin C and Costes M. Aerodynamics of helicopter. Application of the Navier-Stokes codes developed in the framework of the joined German/French CFD research program CHANCE, *CEAS Aerospace Aerodynamics Research Conference*, Cambridge (Great Britain), June 2002.

[2] Gazaix M, Jollès A and Lazareff M. The elsA object-oriented computational tool for industrial applications, *23rd ICAS conference*, Toronto, September 2002.

[3] Bousquet J-M. An overview of applied aerodynamics research at ONERA. *Proceedings of Symposium on Applied Aerodynamics & Design of Aerospace Vehicles*, Bangalore (India), December 2003

[4] Jeanfaivre G, Benoit C and Le Pape M-C. Improvement of the robustness of the Chimera method. *32nd AIAA Fluid Dynamics Conference & Exhibit*, Saint-Louis (USA), June 2002

[5] Cantaloube B and Beaumier P. Simulation of unsteady aero-elastic response of a multi-bladed rotor in forward flight. *27th European Rotorcraft Forum*, Moscou (Russia), September 2001.

[6] Beaumier P, Chelli E and Pahlke K. Navier-Stokes prediction of helicopter rotor performance in hover including aero-elastic effects, *56th American Helicopter Society Forum*, Virginia Beach (USA), May 2000.

[7] Renaud T, Benoit C, Boniface J-C and Gardarein P. Navier-Stokes computations of a complete helicopter configuration accounting for main and tail rotors effects. *29th European Rotorcraft Forum*, Friedrichshaffen (Germany), September 2003.

[8] Gleize V and Costes M, Low-Mach-Number preconditioning applied to turbulent helicopter fuselage flowfield computation. *AIAA Journal*, Vol. 41,No.4, April 2003

[9] Gleize V et al. Helicopter fuselage drag prediction: State of the art in Europe. *39th AIAA Aerospace Sciences Meeting & Exhibit*. Reno (USA), January 2001

[10] Beaumier P and Brezillon J. Numerical Investigation of blade roots (stubs) on hovering rotors, *27th European Rotorcraft Forum*, Moscou (Russia), September 2001.

[11] Le Pape A and Beaumier P. Numerical optimization of helicopter rotor aerodynamic performance in hover. *29th European Rotorcraft Forum*, Friedrichshaffen (Germany), September 2003.

[12] Prieur P and Splettstoesser W. ERATO – an ONERA-DLR Cooperative Programme on Aeroacoustic Rotor Optimisation. *25th European Rotorcraft Forum*, Roma (Italy), September 1999

[13] Altmikus ARM, Wagner S, Beaumier P and Servera G. A comparison: weak versus strong modular coupling for trimmed aero-elastic rotor simulations, *58th American Helicopter Society Forum*, Montreal (Canada), June 2002.